Research Square

Preprints are preliminary reports that have not undergone peer review.
They should not be considered conclusive, used to inform clinical practice,
or referenced by the media as validated information.

A MRI-based nomogram to preoperatively predict histologic grades in stage I endometrial carcinoma

Xiran Jiang
China Medical University
Langyuan Fu
China Medical University
Mingli Zhao
Liaoning Cancer hospital
Jiaqi Zhao
Liaoning Cancer hospital
Jing Song
Shengjing Hospital of China Medical University
Yue Hu
China Medical University
Yue Dong
Liaoning Cancer hospital
Feng Wen (drwenf@126.com)
Shengjing Hospital of China Medical University

Research Article

Keywords: Endometrial carcinoma, histologic grade, MRI, radiomics, nomogram

Posted Date: June 9th, 2022

DOI: https://doi.org/10.21203/rs.3.rs-1675298/v1

License: This work is licensed under a Creative Commons Attribution 4.0 International License. Read Full License

Abstract

Background: This study aims to develop and externally validate a multi-sequence MRI-based radiomics nomogram for preoperatively differentiating low-grade and high-grade tumors in FIGO stage I endometrial carcinoma (EMC).

Methods: A primary cohort was established with a total of 100 patients enrolled from our hospital between Jan. 2017 and Apr. 2021. A consecutively enrolled internal validation cohort (n=41) and an external validation cohort (n=50) were used to test the models. Radiomics features were extracted from T1-weighted contrast-enhanced (T1-CE) and T2-weighted (T2W) MRI and selected with the least absolute shrinkage and selection operator (LASSO) to build the radiomics signature (RS). Clinical factors were analyzed with Mann-Whitney *U* test and Chi-square test. A radiomics nomogram model was constructed incorporating the RS and the most discriminative clinical parameter. Performance of the RS, clinical parameter and nomogram were validated with receiver operating characteristic (ROC), calibration and decision curve analysis (DCA).

Results: The multi-sequence MRI-based RS was built integrating 3 selected features, all from T1-CE MRI. The deep myometrial invasion was considered as the most important clinical parameter (P<0.05). The nomogram model incorporates RS and deep myometrial invasion yielded the best discriminative performance with AUCs of 0.845 (95% confidence interval [CI] 0.759-0.910, SEN=0.900, SPE =0.650), 0.756 (95% CI 0.597-0.876, SEN=0.818, SPE =0.632) and 0.779 (95% CI 0.639-0.884, SEN=0.800, SPE =0.720) in the primary, internal validation and external validation cohorts, respectively. Calibration curves and DCA suggested good potential of our nomogram in clinical uses.

Conclusions: The developed radiomics nomogram can be used as a potential non-invasive tool for preoperatively differentiating low- and high-grade tumors in stage I EMC patients.

Introduction

Endometrial carcinoma (EMC) has been the fourth most common cancer in women globally [1]. The grading of EMC is known as a significant prognostic factor, since the EMC patients with low-grade tumors usually have favorable prognosis with more than 85% 5-year disease-free survival (DFS) rate [2]. While, patients with high-grade tumors are often associated with poor outcomes [3]. Therefore, histopathological assessment of the tumor grade in EMC is crucial for making individual treatment decisions, and guiding the extent of surgery and application of adjuvant treatment [4].

In clinical, routine assignment of the EMC is based on biopsy, curetting specimen or hysterectomy specimen, which are invasive [5]. However, some patients could not accept endometrial biopsy because of cervical stenosis and other reasons, and the limitations of local biopsy could lead to the inconsistent between biopsy pathological results and the final surgical pathological results. Magnetic resonance imaging (MRI) could play a vital role in the preoperative and non-invasive evaluation of EMC [6]. Some functional imaging techniques, such as diffusion-weighted imaging (DWI) and quantitative dynamic contrast-enhanced imaging (DCE), also show some value in the pathological classification of EMC [7,8]. Lower apparent-diffusion-coefficient (ADC) of DWI were observed in the tumor with high grade compared with a low-grade group [7], and low tumor blood flow (Fb) and low rate constant for contrast agent intravasation (kep) of DCE-MRI were associated with high-risk histological subtype and tended to be associated with poor prognosis [8]. While, some studies have concluded that ADC values have no value on identifying pathologic types of EMC [9,10]. Thus, there is still no generally accepted marker in the MRI image can be preoperatively recognized and used for accurate prediction of the pathologic grade for EMC. Therefore, a non-invasive method for early identification of the pathologic grade is urgently needed to help guide treatment strategies in EMCs.

MRI-based radiomics involves high-throughput extraction and quantitative evaluation of huge amounts of features, and has been widely applied in oncology researches [11–17]. Several studies have reported that radiomics features derived from the MRI image can favor the identification of pathologic grades in soft-tissue sarcomas [12,13], breast cancer [14], prostate cancer [15], gliomas [16] and pancreatic neuroendocrine tumor [17]. While, there are only a few studies, to our knowledge, have explored value of radiomics analyses on the histological grades in EMC, and revealed that MRI features can provide information related to the high histological grade (G3 and nonendometriod) EMC [5,18,19]. While, these studies have inherent limitations (e.g. performing analysis based on a single image plane [18,19] and very limited number of features [5,18,19], and used a single MRI sequence of mixed samples with stage I-IV EMCs, and failed to validate their findings in a independent validation set. Besides, the studies only provided numerical results (e.g. AUC values) that cannot be incorporated into clinical practice, which hindered clinical values of the works.

In the present study, we aim to comprehensively analyze conventional MRI sequences and clinical data on the differentiation of pathologic grades in EMC before surgery, and develop and externally validate a clinical-radiomics nomogram for potential clinical applications.

Materials And Methods

Patients

The retrospective study was approved by the ethics committee of our hospital (202104013X). The informed consent form was waived due to the retrospective nature. A total of 100 FIGO stage I EMC patients who underwent T1-CE and T2W MRI were enrolled between Jan. 2017 and Apr. 2021 to be a primary cohort. An internal validation cohort consists of 41 patients were consecutively enrolled in our hospital from Jan. 2017 to Nov. 2021. Fifty patients from another hospital enrolled between Aug. 2017 and Apr. 2021 were used as an external validation cohort. All patients underwent the surgicopathological staging to be graded as low-grade (G1/2) or high-grade (G3 and nonendometriod) EMC according to the FIGO 2009 criteria [20]. The inclusion criteria were as follows: (i) pathologically confirmed stage I EMC: (ii) underwent T1-CE and T2W MR scans two weeks before surgery; and (iii) without any treatment before treatment. The excluding criteria were: (i) harboring other tumor diseases and (ii) the size of the tumor is less than 10 mm. Clinical parameters containing age, body

mass index, cancer antigen 125 (CA-125), deep myometrial invasion, maximum diameters of tumor in three orthogonal planes, menopause, and number of productions were obtained from the medical records.

MRI image acquisition and tumor segmentation

The MRI screenings were performed using a 3.0-T (Vero Siemens) or 1.5-T (General Electric) MRI scanner. The gadoterate meglumine (Gd-DTPA) was used as the contrast agent with the injection dose of 0.1 mmol/kg. In the first center, the T1-CE MRI was scanned with the following parameters: TR/TE = 590ms /11ms, section thickness = 5 mm, gap = 1.25 mm, and matrix = 544mm ×640mm. While, the T2W MRI was scanned with parameters: TR/TE = 677ms /11ms, section thickness = 5 mm, gap = 1 mm, and matrix = 432mm ×640mm. In the second center, parameters for the T1-CE MRI were: TR/TE = 3.4ms /1.32ms, section thickness = 5 mm, gap = 1.5 mm, and matrix = 200mm ×171mm. While, parameters for the T2W MRI were: TR/TE = 4326ms /102ms, section thickness = 5 mm, gap = 1 mm, and matrix = 288mm ×254mm.

A radiological fellow with 4 years of working experience draw the regions of interest (ROIs) slice by slice along the tumor edge in the pelvic sagittal T2WI and T1-CE MRI images, and stored in a NII format. The radiomics feature extraction was performed used the open-source Itk-Snap software (version 3.6.0; www.itksnap.org). In order to assess the feature stability, the tumor segmentation was independently performed by another radiologic fellow, three years of experience on 50 randomly selected patients. The ROI segmentation was under the supervision of a senior radiologist with 16 years of experience to make sure the segmentation was correct. The three readers were blinded to the pathologic results of the patients. Maximum diameters of tumor were measured on the axial, sagittal and coronal T2W MRI separately by two radiological fellows. Two surveyors' results were averaged and used as the final result for statistical analyses. The deep myometrial invasion was evaluated according to the T1-CE and T2W MRI by two radiological fellows. The inconsistent results were determined by a senior radiologist.

Radiomics feature extraction

In total, 3748 radiomics features were calculated from the T1-CE and T2W MRI using the Pyradiomics package (available from url: https://pyradiomics.readthedocs.io/en/latest/index.html) in Python v.3.6. The features included 720 first-order features, 28 shape-based features, 3000 textural features and 3534 filtered features. The textural features contained 960 gray-level co-occurrence matrix (GLCM) features, 640 gray-level run-length matrix (GLRLM) features, 640 gray-level size zone matrix (GLSZM) features, 560 gray-level dependence matrix (GLDM) features and 200 neighborhood gray-tone difference matrix features. The filtered features were calculated from MRI images transformed with eight filters (laplacian of gaussian, square, localbinarypattern2D, exponential, logarithm, gradient, wavelet and squareroot). Details of the procedures for the calculation of radiomics features are described in a previous report [21].

Feature selection and radiomics model development

The selection of radiomics features was performed on the primary cohort to identify reliable and non-redundant features. First, the intraclass correlation coefficient (ICC) analysis was performed to test robustness of all features using 30 randomly selected patients, 15 with low-grade and 15 with high-grade EMC. Features with ICCs over 0.85 were remained. Next, the features were treated with the LASSO regression with 10-fold cross-validation for further selection [22]. Finally, the remained features were selected using the logistic regression with the Akaike Information Criterion (AIC) [23] to develop the radiomics signature (RS). The clinical-radiomics nomogram was constructed incorporating the RS with the most important clinical parameter.

Statistical analysis

All statistical analysis was performed with R language 3.6 (www.rproject.org). Differences of clinical factors between the primary and external cohorts and between the low- and high-grade groups were evaluated with the Mann–Whitney *U* test and *x2* test. The statistical significance level was set at 0.05. ROC curves were plotted using the proc package in R. Calibration curves were plotted using the rms package to evaluate the predictive accuracy of the nomogram. The decision curve analysis (DCA) was employed using the rmda package to evaluate clinical utilities of the developed models.

Results

Patients' characteristics

The primary and external cohorts represented even distributions in patient characteristics (Table 1). The deep myometrial invasion showed significant differences ($P < 0.05$) between the low-grade and high-grade groups in the primary and external cohorts. No significant difference ($P < 0.05$) was found in age, body mass index, CA-125, maximum diameter of tumor, menopause and number of productions.

Table 1
Statistical analysis of patients' characteristics in primary, internal validation and external validation cohorts.

	Primary training (n = 100)			Internal validation (n = 41)			External validation (n = 50)		
	Low-grade (n = 60)	High-grade (n = 40)	*p*	Low-grade (n = 22)	High-grade (n = 19)	*p*	Low-grade (n = 25)	High-grade (n = 25)	*p*
Age (Mean ± SD)	55.50 ± 10.16	58.55 ± 6.70	0.151	51.54 ± 9.79	58.53 ± 11.06	0.362	59.68 ± 8.02	56.96 ± 8.37	0.159
BMI (Mean ± SD)	26.90 ± 3.89	24.46 ± 3.02	< 0.001*	25.25 ± 3.82	24.66 ± 3.50	0.470	24.73 ± 3.47	24.43 ± 2.65	0.392
CA125 (Mean ± SD)	36.47 ± 72.35	22.74 ± 15.50	0.822	100.49 ± 219.41	32.01 ± 21.25	0.340	52.94 ± 69.07	19.44 ± 16.96	0.003*
Tumor transverse diameter (Mean ± SD)	23.90 ± 10.67	22.68 ± 9.10	0.645	28.41 ± 17.97	27.74 ± 14.96	0.391	25.16 ± 9.22	20.64 ± 8.50	0.064
Tumor sagittal diameter (Mean ± SD)	37.65 ± 12.39	34.93 ± 15.99	0.144	31.63 ± 24.58	41.00 ± 22.83	0.434	39.92 ± 16.01	32.44 ± 13.25	0.074
Tumor coronal diameter (Mean ± SD)	34.13 ± 12.57	31.60 ± 10.44	0.486	34.81 ± 19.17	34.89 ± 17.36	0.135	37.64 ± 13.27	29.08 ± 9.45	0.025*
Uterus transverse diameter (Mean ± SD)	43.78 ± 12.16	52.05 ± 47.53	0.762	59.86 ± 16.11	59.53 ± 15.84	0.505	44.28 ± 10.14	40.00 ± 8.24	0.137
Uterus sagittal diameter (Mean ± SD)	56.05 ± 16.24	52.35 ± 11.61	0.211	61.86 ± 22.37	68.16 ± 24.91	0.372	57.84 ± 15.49	50.40 ± 13.98	0.041*
Uterus corona diameter (Mean ± SD)	51.15 ± 12.09	51.75 ± 11.06	0.725	65.13 ± 15.47	66.11 ± 17.59	0.373	56.64 ± 11.87	48.84 ± 8.82	0.024*
Transverse diameter ratio (Mean ± SD)	0.55 ± 0.18	0.51 ± 0.19	0.357	0.46 ± 0.23	0.59 ± 0.19	0.426	0.57 ± 0.15	0.52 ± 0.18	0.295
Sagittal diameter ratio (Mean ± SD)	0.68 ± 0.18	0.66 ± 0.22	0.425	0.47 ± 0.22	0.53 ± 0.19	0.383	0.68 ± 0.15	0.64 ± 0.15	0.443
Coronal diameter ratio (Mean ± SD)	0.66 ± 0.13	0.62 ± 0.18	0.479	0.51 ± 0.21	0.46 ± 0.19	0.470	0.66 ± 0.17	0.59 ± 0.14	0.088
Number of pregnancies, n (%)			0.056			0.043*			0.254
<3	40 (66.7%)	19 (47.5%)		14 (63.6%)	6 (31.6%)		9 (36.0%)	13 (52.0%)	
≥ 3	20 (33.3%)	21 (52.5%)		8 (36.4%)	13 (68.4%)		16 (64.0%)	12 (48.0%)	
Number of miscarriages, n (%)			0.084			0.529			0.015*
<2	47 (78.3%)	25 (62.5%)		17 (77.3%)	13 (68.4%)		13 (52.0%)	21 (84.0%)	
≥ 2	13 (21.7%)	15 (37.5%)		5 (22.7%)	6 (31.6%)		12 (48.0%)	4 (16.0%)	
Menopause, n (%)			0.104			0.987			0.649
No	49 (81.7%)	27 (67.5%)		7 (31.8%)	6 (31.6%)		21 (84.0%)	21 (84.0%)	
Yes	11 (18.3%)	13 (32.5%)		15 (68.2%)	13 (68.4%)		4 (16.0%)	4 (16.0%)	
Deep myometrial invasion, n (%)			0.001*			0.006*			0.048*
No	41 (68.3%)	14 (35.0%)		20 (90.9%)	10 (52.6%)		9 (36.0%)	16 (64.0%)	
Yes	19 (31.7%)	26 (65.5%)		2 (9.1%)	9 (47.4%)		16 (64.0%)	9 (36.0%)	
Number of productions, n (%)			0.143			0.101			0.018*
<2	43 (71.7%)	23 (57.5%)		16 (72.7%)	9 (47.4%)		12 (48.0%)	20 (75.0%)	
≥ 2	17 (28.3%)	17 (42.5%)		6 (27.3%)	10 (52.6%)		13 (52.0%)	5 (25.0%)	

SD: standard deviation; CA 125: cancer antigen 125; BMI: body mass index; *, $P < 0.05$.

Features selection and radiomics signature development

A total of 3 features were selected as the most predictive features with the LASSO logistic regression (Fig. 1), all from the T1-CE MRI. Table 2 listed the prediction capability of each selected feature. The features showed statistical significances ($P < 0.05$) between the low- and high-grade groups in both primary and external cohorts. Boxplots and results of the unsupervised cluster analysis of the selected features were shown in Fig. 2 and Fig. 3, respectively. By integrating the features with the corresponding coefficients, the formula of RS was developed and shown as following:

Radiomics signature (RS) = -25.41778 + 21.87112 × wavelet-LHH_glcm_Idn + 0.03477 × wavelet-HLL_glrlm_LongRunHighGrayLevelEmphasis + 1.44688 × log-sigma-3-0-mm-3D_glcm_SumEntropy

As depicted in Fig. 4, most patients represent obvious differences of RS values between the low-grade and high-grade groups, which indicated that the patients with different pathological grades can be roughly differentiated by the RS.

Table 2
Prediction performance of the selected radiomics features.

Feature	Cohort	Mean ± SD		AUC	*P*
		Low-grade	**High-grade**		
wavelet-LHH_glcm_Idn	Primary training	0.878 ± 0.030	0.900 ± 0.016	0.721	< 0.001
	Internal validation	0.892 ± 0.263	0.892 ± 0.278	0.424	0.834
	External validation	0.888 ± 0.285	0.858 ± 0.032	0.741	0.030
wavelet-HLL_glrlm_LongRunHighGrayLevelEmphasis	Primary training	35.300 ± 19.217	56.129 ± 21.484	0.750	< 0.001
	Internal validation	42.60 ± 38.374	52.787 ± 28.315	0.631	0.007
	External validation	63.954 ± 27.822	53.360 ± 19.548	0.571	0.388
log-sigma-3-0-mm-3D_glcm_SumEntropy	Primary training	2.490 ± 0.464	0.431 ± 1.056	0.756	< 0.001
	Internal validation	2.652 ± 0.538	2.912 ± 0.432	0.621	0.025
	External validation	3.253 ± 0.418	3.099 ± 0.437	0.608	0.190

SD, standard deviation.

Development and validation of the radiomics nomogram

The deep myometrial invasion was considered as the most discriminative clinical parameter ($P < 0.05$), and integrated with the RS to build a radiomics nomogram. As shown in Fig. 5A, the developed nomogram contains the deep myometrial invasion in the second row and RS in the third row. Calibration curves demonstrated favorable calibrations of the nomogram-predicted and actual values in the primary (Fig. 5B), internal validation (Fig. 5C) and external validation(Fig. 5D) cohorts.

Radiomics models evaluation

Discrimination performance of the RS, deep myometrial invasion and nomogram on both primary and external cohorts were compared and shown in Fig. 6 and Table 3. The nomogram achieved the best performance among the three models in regard to AUC, accuracy and sensitivity. The Delong test's results revealed significant differences between the deep myometrial invasion and nomogram on both primary and external cohorts. DCA curves were depicted in Fig. 7, showing that more benefits can be obtained by using the nomogram compared with the deep myometrial invasion or RS.

Table 3
Comparisons of the deep myometrial invasion, RS and nomogram.

	Primary					Internal validation					External validation				
	AUC (95% CI)	Acc	Sen	Spe	P	AUC (95% CI)	Acc	Sen	Spe	P	AUC (95% CI)	Acc	Sen	Spe	P
M1	0.667 (0.565–0.758)	0.670	0.683	0.650		0.691 (0.528–0.826)	0.707	0.909	0.474		0.640 (0.492–0.771)	0.640	0.640	0.640	
M2	0.833 (0.746–0.900)	0.780	0.767	0.800		0.725 (0.563–0.852)	0.707	0.773	0.632		0.758 (0.617–0.868)	0.740	0.680	0.800	
M3	0.845 (0.759–0.910)	0.800	0.900	0.650		0.756 (0.597–0.876)	0.731	0.818	0.632		0.779 (0.639–0.884)	0.760	0.800	0.720	
M1 vs. M2					0.005*					0.716					0.198
M1 vs. M3					< 0.001*					0.393					0.045*
M2 vs. M3					0.529					0.199					0.480

M1, Deep myometrial invasion; M2, RS; M3, Nomogram.

Discussion

This study supports the promising role of MRI-based radiomics for accurate and preoperative histologic grading in FIGO stage I EMC. The developed RS combining T1-CE and T2W MRI generated good prediction performance with AUCs ranging from 0.725 to 0.833 in the primary and external validation cohorts. While, previous studies only evaluated very limited number of features (5 [19], 15 [5] and 180 [18] features in total) from samples with mixed stage I-IV EMCs, and validate their findings in the same dataset, which had inherent limitations. In this study, we analyzed 3748 radiomics features from the two MRI sequences and identified 3 features as the most important predictors and validated in the external cohort. All features belong to the textural feature class, which can reflect information regarding the intra-tumor heterogeneity and gray distribution [24]. Our findings suggested that the heterogeneity within EMC was highly associated with the histologic grades, and was consistent with previous works that also found texture features were predictive on the histological grades in EMC [5,18]. Since our selected features were all derived from transformed images, which may explained why the differentiation of histological grades in stage I EMC via visual assessments on the MRI image is very poor. Besides, the most important features were all from T1-CE MRI, with no features remained from the T2W MRI after the feature selection, which indicate that T1-CE may hold more discriminative information related to the histologic grades compared to T2W.

We found the deep myometrial invasion is a predictive clinical parameter for the histologic grading in EMC. This was not reported before our work. When the deep myometrial invasion was used alone, the predictive AUCs ranged from 0.640 to 0.691 in the primary and external cohorts. When comparing the deep myometrial invasion with the nomogram model, we found significant differences in their diagnostic performance ($P < 0.05$), which indicated that the deep myometrial invasion can add complementary information to the nomogram. Preoperative tumor measurements based on MRI may potentially predict preoperative deep myometrial invasion and high risk pathological type in EMC [25,26]. There was no difference in the size of the lesion between two different pathological grades in the study, which may be related to the fact that the patients included in this study were all I stage patients with relatively small lesions confined to the uterus. Fasmer et al also found that tumor volume yielded significantly lower AUC compared to the whole-tumor radiomic signatures for high-grade endometrioid tumors [27].

Previous studies related to our work only provided ROC curves and AUCs which cannot be incorporated into clinical practice [5,18,19]. While, we constructed a clinical-radiomics nomogram incorporating the RS and deep myometrial invasion, and yielded the best prediction performance ranging from 0.756 to 0.845 on the primary and external cohorts. This was higher than previous reported AUCs on for the G3 EMC ranging from 0.630 to 0.830, partially because they failed to integrate clinical factors into their models [5,18,19]. The specificity of our nomogram was also improved compared with the RS or deep myometrial invasion alone. DCA analysis confirmed clinical usefulness of the nomogram over a wide range of threshold probabilities. To use our nomogram, clinicians need to calculate the RS value for a patient using the proposed formula, then integrate the value with the deep myometrial invasion status to calculate possibilities of being low-grade or high-grade according to the nomogram.

There are limitations in this study. First, although this is a multi-center study, the number of samples was still relative small, due to the data collecting challenges. Our findings would be confirmed in larger studies. Second, in ACR and IKNC DWI imaging is recommended as standard for endometrium carcinoma, but we only evaluated T1-CE and T2W MRI data because some patients did not underwent DWI sequence, and values of other MRI sequences on the prediction of pathologic grades in EMC should be studied in the next prospective study. Third, the patients were separated into a G1/2 and a G3/nonendometriod group. A future investigation to classify G1 and G2 groups is needed to guide personalized treatment strategies. Finally, manual

segmentations of ROIs in the MRI slices were time-consuming for the radiologists involved in this study. Automated mask segmentation algorithms (e.g. deep neural networks) would be addressed to decrease workload.

Conclusions

This study revealed values of MRI-based radiomics features from conventional sequences on the pathologic grades in FIGO stage I EMC. The developed nomogram can be considered as a potential tool for non-invasive assessments and tailored treatment strategies in EMC.

Abbreviations

EMC
Endometrial carcinoma
DWI
diffusion-weighted imaging
DCE
dynamic contrast-enhanced imaging
AUC
Area under the Curve
MRI
Magnetic resonance imaging
DCA
decision curve analysis
LASSO
Least absolute shrinkage and selection operator
ROC
Receiver-Operating-Characteristic
Glszm
gray level size zone matrix
glrlm
gray level run length matrix
glcm
gray level co-occurrence matrix
SD
standard deviation
CA 125
cancer antigen 125
BMI
body mass index
M1, Deep myometrial invasion
M2, RS
M3, Nomogram.

Declarations

Ethics approval and consent to participate

All analyses of human data conducted in this study were approved by the Institutional Review Board of the Cancer Hospital of China Medical University and in accordance with the ethical standards of the institutional and/or national research committee and with the 1964 Helsinki declaration and its later amendments or comparable ethical standards. The need for informed consent was waived by the ethics committee of Liaoning Cancer Hospital and Institute in view of the retrospective nature of the analysis and the anonymity of the data.

Consent for publication

Not applicable.

Availability of data and materials

The datasets used and/or analysed during the current study are available from the corresponding author on reasonable request.

Competing interests

No conflicts of interest.

Funding

Not applicable.

Authors' contributions

XJ contributed to study concepts and manuscript preparation. XJ contributed to study design. YD and FW contributed to data acquisition. LF contributed to quality control of data and algorithms. LF contributed to data analysis and interpretation. LF contributed to statistical analysis. XJ contributed to manuscript review. All authors read and approved the final manuscript.

Acknowledgements

The study was supported by Climbing Fund of National Cancer Center (NCC201806B011), Special Foundation for the Central Government Guides the Development of Local Science and Technology of Liaoning Province (2018416029), The Fundamental Research Funds for the Central University (LD202119) and China National Natural Science Foundation (31770147).

Authors' information

XJ and LF are co-first authors.[1]School of Intelligent Medicine, China Medical University, Liaoning, China, 110122, P.R. China[2]Department of Radiology, Cancer Hospital of China Medical University, Cancer Hospital of Dalian University of Technology, Liaoning Cancer Hospital and Institute, Liaoning, China, 110042, P.R. China [3]Department of Radiology, Shengjing Hospital of China Medical University, Shenyang, China, 110122, P.R. China

References

1. Siegel RL, Miller KD, Jemal A (2019) Cancer statistics. CA Cancer J Clin, 69: 7–34.
2. Huvila J, Pors J, Thompson EF, Gilks CB (2021). Endometrial carcinoma: molecular subtypes, precursors and the role of pathology in early diagnosis. J Pathol, 253: 355–365. doi: 10.1002/path.5608.
3. Cancer Genome Atlas Research Network, Kandoth C, Schultz N, Cherniack AD, Akbani R, Liu Y, Shen H, Robertson AG, Pashtan I, Shen R, Benz CC, Yau C, Laird PW, Ding L, Zhang W, Mills GB, Kucherlapati R, Mardis ER, Levine DA. (2013). Integrated genomic characterization of endometrial carcinoma. Nature, 497: 67–73. doi: 10.1038/nature12113.
4. Kommoss F, Kommoss F, Grevenkamp F, Bunz AK, Taran FA, Fend F, Brucker SY, Wallwiener D, Schönfisch B, Greif K, Lax S, Staebler A, Kommoss S(2017). L1CAM: amending the "low-risk" category in endometrial carcinoma. J Cancer Res Clin Oncol,143(2):255–262. doi: 10.1007/s00432-016-2276-3.
5. Fasmer KE, Hodneland E, Dybvik JA, Wagner-Larsen K, Trovik J, Salvesen Ø, Krakstad C, Haldorsen HIS (2021). Whole-Volume Tumor MRI Radiomics for Prognostic Modeling in Endometrial Cancer. J Magn Reson Imaging, 53: 928–937. doi: 10.1002/jmri.27444.
6. Haldorsen IS, Salvesen HB (2016). What is the best preoperative imaging for endometrial cancer? Curr Oncol Rep, 18:1–11. doi: 10.1007/s11912-016-0506-0.
7. Zhang Q, Ouyang H, Ye F, Chen S, Xie L, Zhao X, Yu X. Multiple mathematical models of diffusion-weighted imaging for endometrial cancer characterization: Correlation with prognosis-related risk factors. Eur J Radiol 2020; 130: 109102.
8. Fasmer KE, Bjørnerud A, Ytre-Hauge S, Grüner R, Tangen IL, Werner HM, Bjørge L, Salvesen Ø O, Trovik J, Krakstad C, Haldorsen IS. Preoperative quantitative dynamic contrast-enhanced MRI and diffusion-weighted imaging predict aggressive disease in endometrial cancer. Acta Radiol 2018; 59: 1010–1017.
9. Rechichi G, Galimberti S, Signorelli M, Franzesi CT, Perego P, Valsecchi MG, Sironi S.Endometrial cancer: correlation of apparent diffusion coefficient with tumor grade, depth of myometrial invasion, and presence of lymph node metastases. AJR Am J Roentgenol 2011; 197: 256–262.
10. Bonatti M, Pedrinolla B, Cybulski AJ, Lombardo F, Negri G, Messini S, Tagliaferri T, Manfredi R, Bonatti G. Prediction of histological grade of endometrial cancer by means of MRI. Eur J Radiol 2018; 103: 44–50.
11. Rogers W, Thulasi Seetha S, Refaee TAG, Lieverse RIY, Granzier RWY, Ibrahim A, Keek SA, Sanduleanu S, Primakov SP, Beuque MPL, Marcus D, van der Wiel AMA, Zerka F, Oberije CJG, van Timmeren JE, Woodruff HC, Lambin P (2020). Radiomics: from qualitative to quantitative imaging. Br J Radiol, 93: 20190948. doi: 10.1259/bjr.20190948.
12. Crombé A, Marcellin PJ, Buy X, Stoeckle E, Brouste V, Italiano A, Le Loarer F, Kind M (2019). Soft-Tissue Sarcomas: Assessment of MRI Features Correlating with Histologic Grade and Patient Outcome. Radiology, 291: 710–721. doi: 10.1148/radiol.2019181659.
13. Wang H, Chen H, Duan S, Hao D, Liu J.J (2020). Radiomics and Machine Learning With Multiparametric Preoperative MRI May Accurately Predict the Histopathological Grades of Soft Tissue Sarcomas. J Magn Reson Imaging, 51: 791–797. doi: 10.1002/jmri.26901.
14. Santucci D, Faiella E, Cordelli E, Calabrese A, Landi R, de Felice C, Beomonte Zobel B, Grasso RF, Iannello G, Soda P (2021). The Impact of Tumor Edema on T2-Weighted 3T-MRI Invasive Breast Cancer Histological Characterization: A Pilot Radiomics Study.
15. Cancers (Basel),13:4635. doi: 10.3390/cancers13184635.
16. Gong L, Xu M, Fang M, Zou J, Yang S, Yu X, Xu D, Zhou L, Li H, He B, Wang Y, Fang X, Dong D, Tian J (2020). Noninvasive Prediction of High-Grade Prostate Cancer via Biparametric MRI Radiomics. J Magn Reson Imaging, 52: 1102–1109. doi: 10.1002/jmri.27132.
17. Park YW, Choi YS, Ahn SS, Chang JH, Kim SH, Lee SK (2019) Radiomics MRI Phenotyping with Machine Learning to Predict the Grade of Lower-Grade Gliomas: A Study Focused on Nonenhancing Tumors. Korean J Radiol 2019; 20: 1381–1389. doi: 10.3348/kjr.2018.0814.
18. Lotfalizadeh E, Ronot M, Wagner M, Cros J, Couvelard A, Vullierme MP, Allaham W, Hentic O, Ruzniewski P, Vilgrain V (2017). Prediction of pancreatic neuroendocrine tumour grade with MR imaging features: added value of diffusion-weighted imaging. Eur Radiol 2017; 27: 1748–1759. doi:

10.1007/s00330-016-4539-4.

19. Ueno Y, Forghani B, Forghani R, Dohan A, Zeng XZ, Chamming's F, Arseneau J, Fu L, Gilbert L, Gallix B, Reinhold C (2017). Endometrial Carcinoma: MR Imaging-based Texture Model for Preoperative Risk Stratification-A Preliminary Analysis. Radiology, 284: 748–757. doi: 10.1148/radiol.2017161950.
20. Ytre-Hauge S, Dybvik JA, Lundervold A, Salvesen ØO, Krakstad C, Fasmer KE, Werner HM, Ganeshan B, Høivik E, Bjørge L, Trovik J, Haldorsen IS (2018). Preoperative Tumor Texture Analysis on MRI Predicts High-Risk Disease and Reduced Survival in Endometrial Cancer. J Magn Reson Imaging 2018; 48: 1637–1647. doi: 10.1002/jmri.26184.
21. Pecorelli (2009). Revised FIGO staging for carcinoma of the vulva, cervix, and endometrium. Int J Gynaecol Obstet,105: 103–104. doi: 10.1016/j.ijgo.2009.02.012.
22. van Griethuysen JJM, Fedorov A, Parmar C, Hosny A, Aucoin N, Narayan V, Beets-Tan RGH, Fillion-Robin JC, Pieper S, Aerts HJWL (2017). Computational Radiomics System to Decode the Radiographic Phenotype. Cancer Res, 77(21):e104-e107. doi: 10.1158/0008-5472.CAN-17-0339.
23. R. Tibshirani (1997). The lasso method for variable selection in the Cox model. Stat Med, 16: 385–395. doi: 10.1002/(sici)1097-0258(19970228)16:4<385::aid-sim380>3.0.co;2-3.
24. Pan W (2021). Akaike's information criterion in generalized estimating equations. Biometrics, 57: 120–125. doi: 10.1111/j.0006-341x.2001.00120.x.
25. P. Afshar, A. Mohammadi, K. N. Plataniotis, A Oikonomou, H Benali (2019). From Hand-Crafted to Deep Learning-Based Cancer Radiomics: Challenges and Opportunities. IEEE Signal Process, 36: 132–160. **doi: 10.1109/MSP.2019.2900993**
26. Ytre-Hauge S, Husby JA, Magnussen IJ, Werner HM, Salvesen ØO, Bjørge L, Trovik J, Stefansson IM, Salvesen HB, Haldorsen IS (2015). Preoperative tumor size at MRI predicts deep myometrial invasion, lymph node metastases, and patient outcome in endometrial carcinomas. Int J Gynecol Cancer, 25: 459–466. doi: 10.1097/IGC.0000000000000367.
27. Keles DK, Evrimler S, Merd N, Erdemoglu E. Endometrial cancer: the role of MRI quantitative assessment in preoperative staging and risk stratification. Acta Radiol. 2021 Jun 29;2841851211025853. doi: 10.1177/02841851211025853.
28. Fasmer KE, Hodneland E, Dybvik JA, Wagner-Larsen K, Trovik J, Salvesen Ø, Krakstad C, Haldorsen IHS.Whole-Volume Tumor MRI Radiomics for Prognostic Modeling in Endometrial Cancer. J Magn Reson Imaging. 2021;53(3):928–937. doi: 10.1002/jmri.27444.

Figures

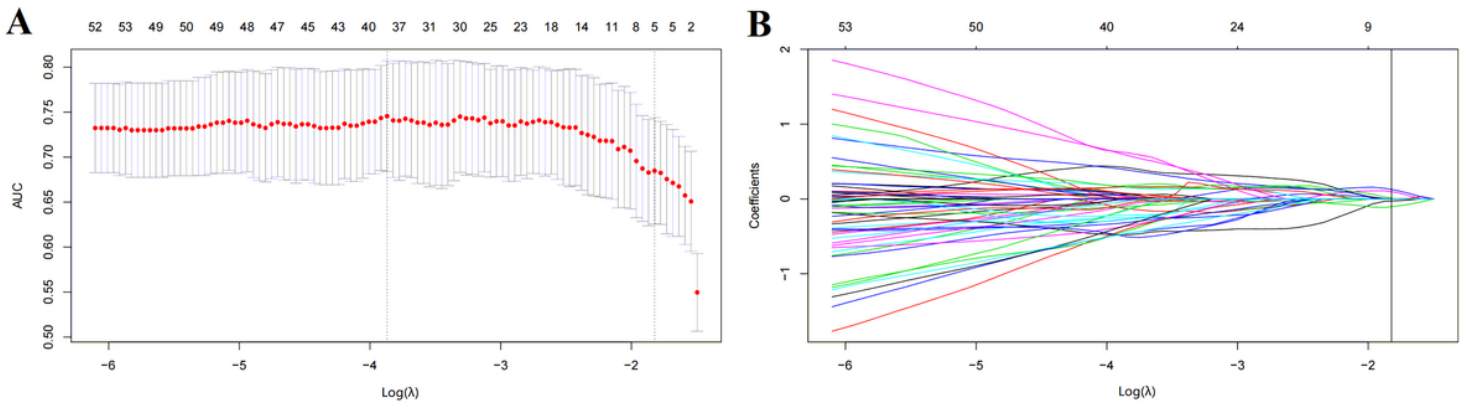

Figure 1

Radiomics feature selection using the LASSO algorithm. (A) Selection of the tuning parameter λ with 10-fold cross-validation based on the minimum criteria. The optimal λ and log (λ) were 0.1615989 and -1.822638, respectively. (B) LASSO coefficient profiles of the radiomics features.

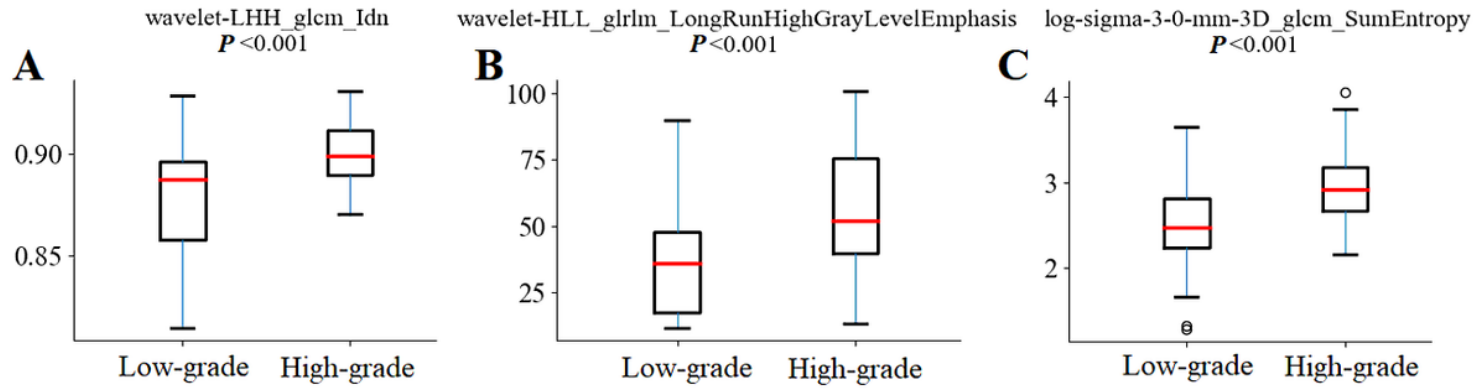

Figure 2

Boxplots of the selected radiomics features. (A) wavelet-LHH_glcm_Idn. (B) wavelet-HLL_glrlm_LongRunHighGrayLevelEmphasis. (C) log-sigma-3-0-mm-3D_glcm_SumEntropy. The x-axis represents the low-grade and high-grade groups, whereas the y-axis indicates values of the features.

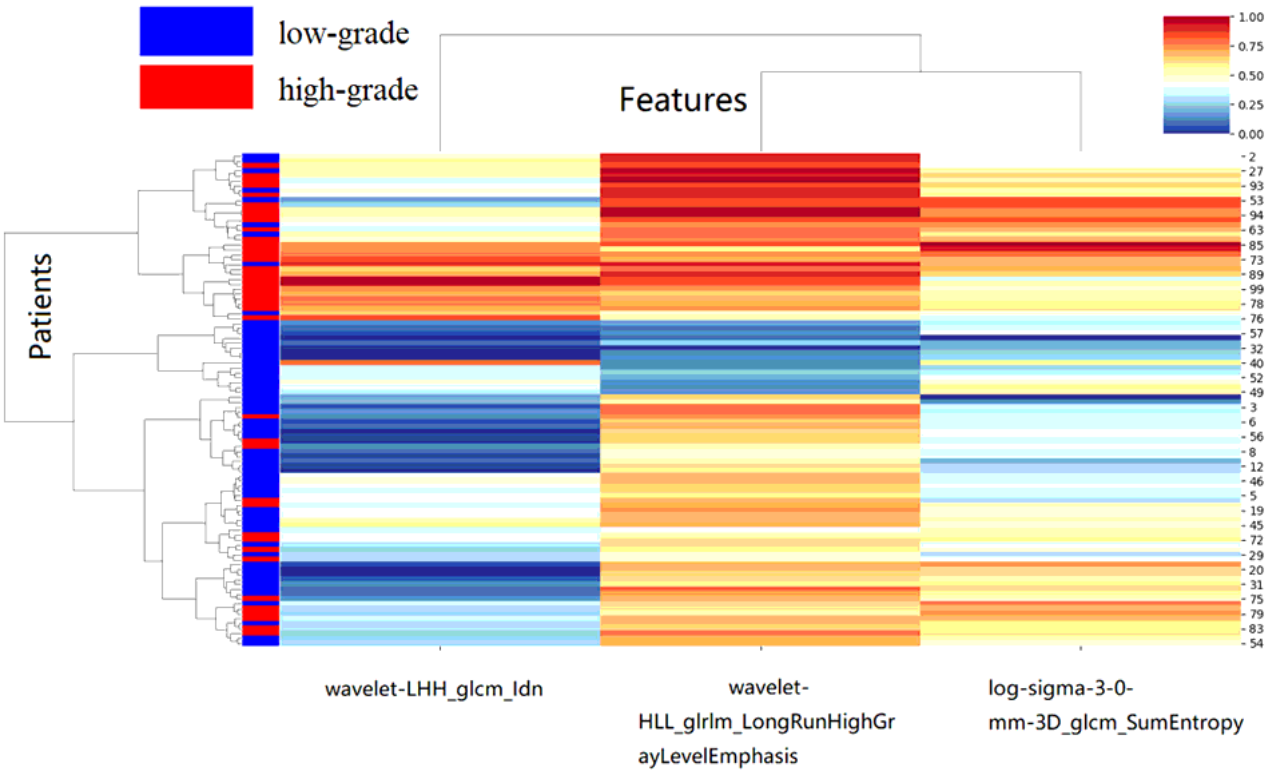

Figure 3

Unsupervised clustering of the selected features and all EMC patients. The *x* axis indicates the features, whereas the *y* axis indicates the patients. The blue color shows low-grade patients, whereas the red color shows high-grade patients. The color coding indicates normalized values of the features.

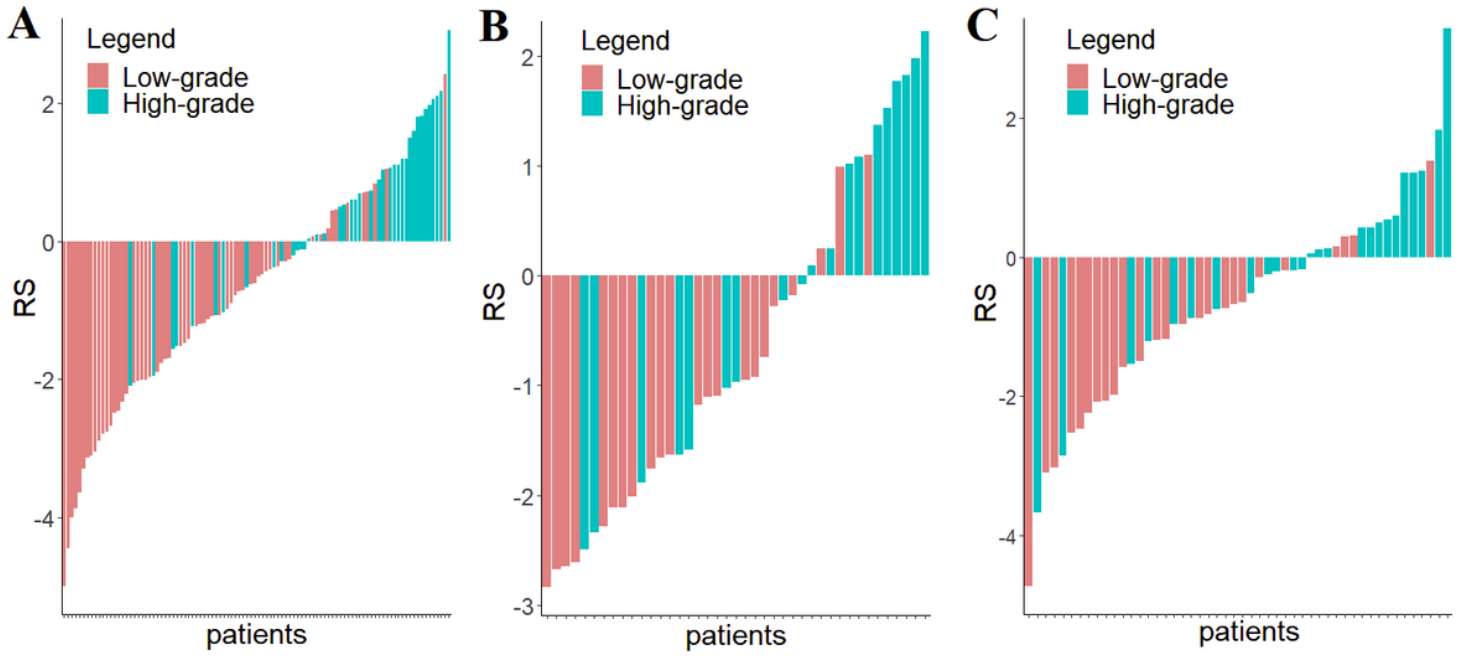

Figure 4

The developed multi-sequence MRI-based RS for differentiating low-grade and high-grade EMCs in the primary training (A), internal validation (B) and external validation (C) cohorts. The red bars indicate low-grade patients, whereas the green bars indicate high-grade patients.

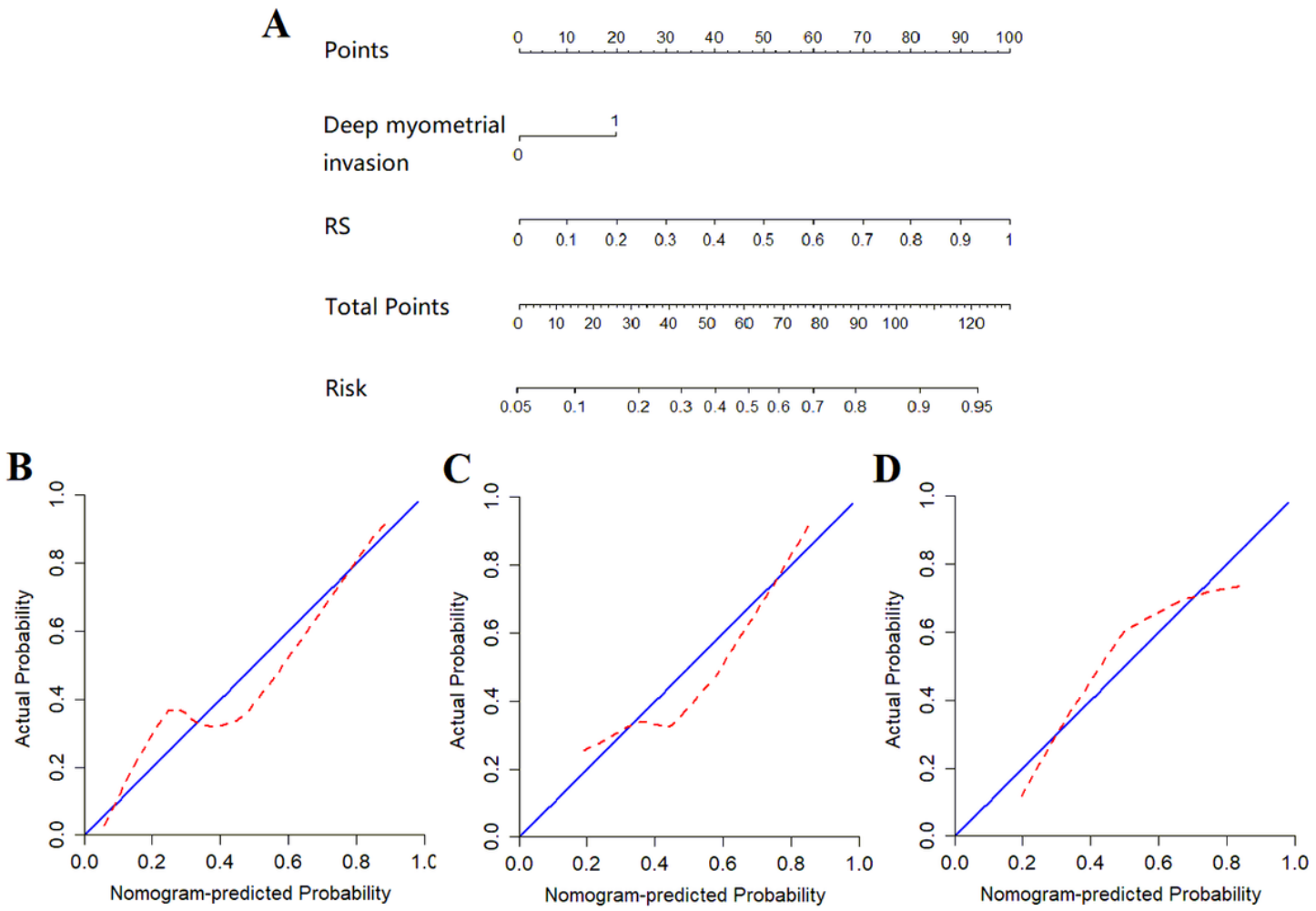

Figure 5

The radiomics nomogram for preoperative predicting the histologic grade of stage I EMC. (A) The nomogram integrating RS and deep myometrial invasion. (B), (C) and (D), calibration curves of the nomogram in the primary training (B), internal validation (C) and external validation (D) cohorts.

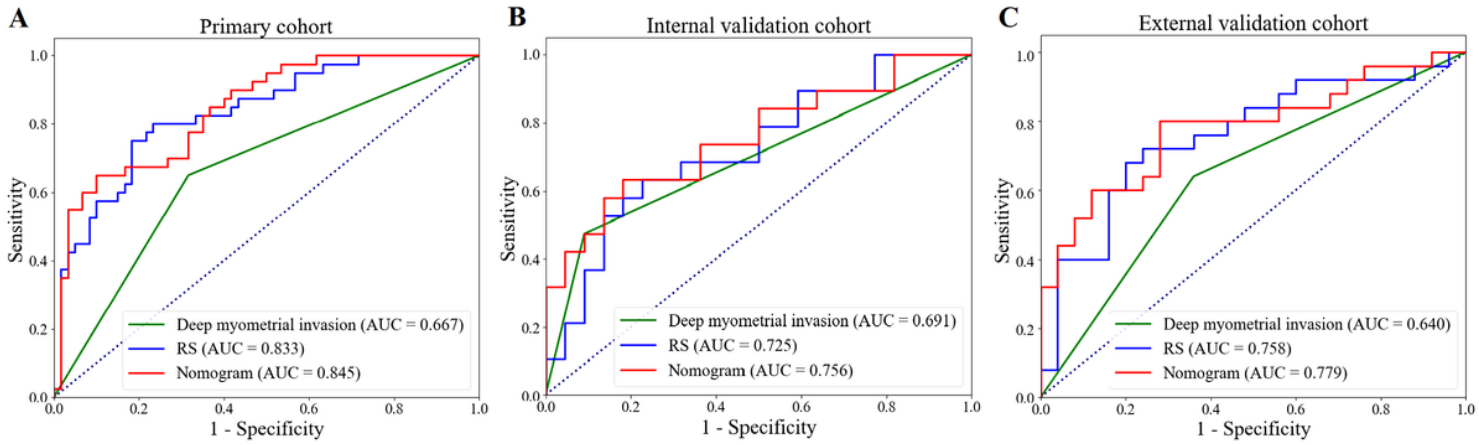

Figure 6

ROC curves of the developed radiomics models in the primary training (A), internal validation (B) and external validation (C) cohorts.

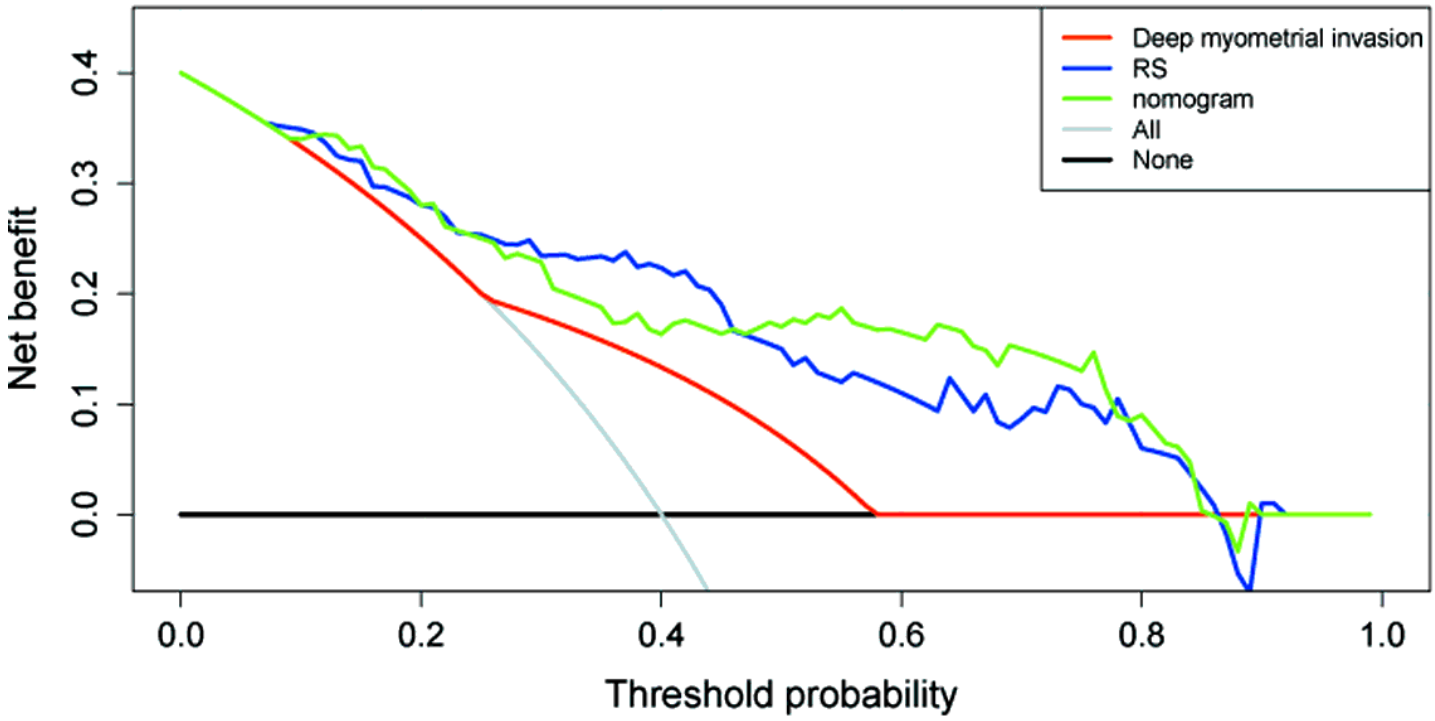

Figure 7

DCA curves of the developed radiomics models. The black line indicates the assumption that all patients were with low-grade EMC. The blue line indicates the assumption that all patients were with high-grade EMC. The red, blue and green lines represent the RS, deep myometrial invasion and nomogram, respectively.

Supplementary Files

This is a list of supplementary files associated with this preprint. Click to download.

- table1.docx
- table2.docx
- table3.docx